MOLECULAR PHYSICS, 1976, VOL. 32, NO. 2, 555–567

40

Observation of the rubidium-85, -87 solid-state hyperfine structure anomaly by electron spin resonance spectroscopy

by RON CATTERALL
Department of Chemistry and Applied Chemistry, Salford University, Salford M54 WT, England
and PETER P. EDWARDS†
Department of Chemistry, Cornell University, Ithaca, New York 14853, U.S.A.

(*Received* 25 *March* 1976)

The rubidium-85, -87 hyperfine structure anomaly for rubidium ' atomic-like ' impurity states in a host matrix (hexamethylphosphoramide) has been measured by electron spin resonance spectroscopy. The average value $[(1{\cdot}672 \pm 0{\cdot}8) \times 10^{-3}]$ for an impurity state with approximately 70 per cent rubidium-5*s* atomic character is in *overall* agreement with the experimental value $[(3{\cdot}515 \pm 0{\cdot}004) \times 10^{-3}]$ for gas-phase rubidium atoms with 100 per cent occupancy of the 5*s* orbital. It is emphasized that, disregarding any enhanced mixing of higher angular momentum ($L > 0$) states in the matrix-bound state, the behaviour of the unpaired electron at (or inside) the nucleus is the same irrespective of whether the atom is in the gas phase or embedded in a host matrix. The slight decrease in the measured hyperfine structure anomaly for the solid-state species, as compared with its gas-phase counterpart, is reconciled with an appreciable admixture of rubidium 5p character into the impurity atom ground state wavefunction.

1. INTRODUCTION

For atoms in the $^2S_{1/2}$ state, the magnetic hyperfine interaction constant, a, is given by the Fermi–Segré formula [1–3]

$$a = \frac{8\pi}{3}\left(\frac{\mu_I}{I}\right)\mu_N|\psi(0)|^2, \tag{1}$$

where μ_I is the nuclear magnetic moment in units of the nuclear magneton, μ_N, and $|\psi(0)|^2$ is the square of the modulus of the normalized electronic wavefunction at the nucleus. The theory [1] on which equation (1) is based treats the nucleus as a point dipole of negligible size and infinite mass. Under these assumptions, one might expect that the ratio of the hyperfine splittings for two isotopes of the same electronic state would be

$$\frac{a_1}{a_2} = \left(\frac{\mu_{I_1}}{\mu_{I_2}}\right)\left(\frac{I_2}{I_1}\right), \tag{2}$$

that is $|\psi(0)|^2$ is tacitly assumed to be identical for the two isotopic states.

† British Fulbright Scholar 1975–1977.

Experimental studies of alkali atoms in the gas phase have shown deviations from this equality. Bitter [4] first pointed out in the case of rubidium-85 and rubidium-87 isotopes that if the finite size of the respective nuclei were taken into account, a will depend explicitly upon the spatial distribution of the nuclear magnetism, and equation (2) must be replaced by [4]

$$\frac{a_1}{a_2}=\left(\frac{\mu_{I_1}}{\mu_{I_2}}\right)\left(\frac{I_2}{I_1}\right)(1+{}_1\Delta_2), \tag{3}$$

where ${}_1\Delta_2$, defined as the hyperfine structure anomaly, depends on the particular details of the nuclear structures of isotopes 1 and 2.

The rubidium-85, -87 hyperfine structure anomaly, ${}_{85}\Delta_{87}$, in gas-phase rubidium atoms has been measured [5, 6] by atomic-beam spectroscopy at $(3{\cdot}515 \pm 0{\cdot}004) \times 10^{-3}$. More recently DeLange and Monster [7] have reported forbidden electron resonance transitions in gaseous rubidium atoms. From their experimental results, we calculate ${}_{85}\Delta_{87}=3{\cdot}517 \times 10^{-3}$, in good agreement with the value obtained from atomic beam spectroscopy.

Thus, so far, measurements of the hyperfine structure anomaly for rubidium atoms (and indeed all of the alkali atoms) have been confined solely to atoms in the *gas phase* in which the occupancy of the rubidium-5*s* orbital is necessarily 100 per cent. In this communication we report the observation, by electron spin resonance (E.S.R.) spectroscopy, of the rubidium-85, -87 *solid-state* hyperfine structure anomaly associated with rubidium, atomic-like, impurity states in the matrix hexamethylphosphoramide (HMPA). In this instance, the observation of a hyperfine structure anomaly is made even more interesting by the fact that *ca.* 40 per cent of the rubidium-5*s* electron (spin) density is delocalized onto the surrounding matrix.

2. Experimental section

Rubidium–HMPA solutions were prepared in both quartz and Pyrex vessels using standard high vacuum techniques [8]. The blue solutions (*ca.* 0·1 M† in metal) were rapidly frozen to 77 K to form homogeneous blue solids.

Electron spin resonance spectra were recorded at *ca.* 9·1 GHz on a Varian V4502 spectrometer. Magnetic field, microwave frequency, and temperature were controlled and measured using standard accessories.

3. Experimental results

3.1. *Electron spin resonance spectra*

Spectra (figure 1 (*a*)) from samples prepared and examined in quartz cells consisted of a strong, isotropic sextet, arising from hyperfine interaction between an unpaired electron and a single rubidium-85 nucleus, and three weaker resonances associated with the less abundant rubidium-87 nucleus. In Pyrex cells, the low-field members‡ [$m_I=+\frac{3}{2}\{(2, 2)\leftarrow(1, 1)\}$, $m_I=+\frac{1}{2}\{(2, 1)\leftarrow(1, 0)\}$]

† 0·1 M ≡ 0·1 mol dm^{-3}.

‡ We refer to individual resonances by the value of m_I (high-field notation) followed by a precise description using F, m_F $\{(F', m_{F'})\leftarrow(F'', m_{F''})\}$ values of the appropriate magnetic energy levels (see figures 2 (*a*) and 2 (*b*)).

of the rubidium-87 quartet were obscured by an intense resonance at $g \sim 4$ arising from paramagnetic impurities in the glass. Otherwise spectra were identical from samples prepared and examined in either quartz or Pyrex systems. In all instances, the rubidium-87, $m_I = -\frac{1}{2}\{(2, 0) \leftarrow (1, -1)\}$ line was obscured by a strong singlet resonance occuring close to the free-spin region (*ca.* 3200 G).

Spectra recorded at high machine amplification showed several, weaker multiplet resonances, and our identification of lines from both rubidium-85

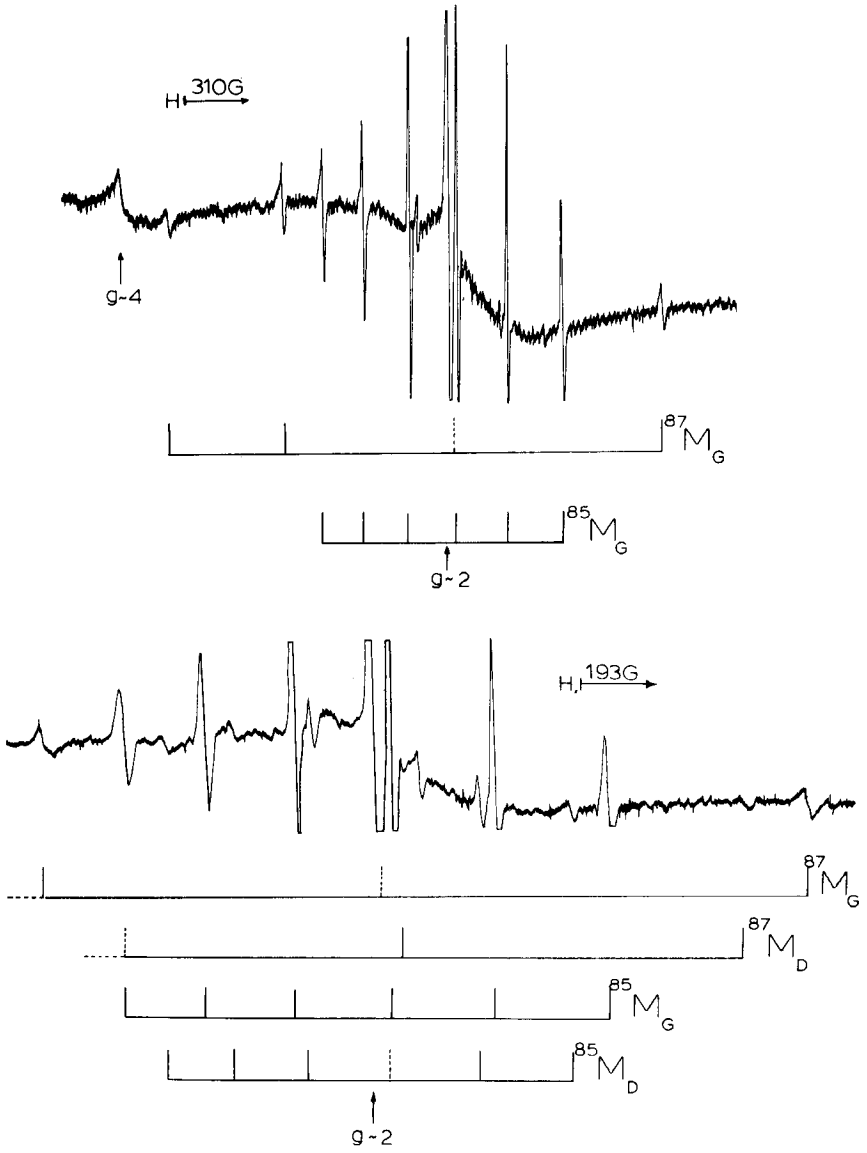

Figure 1. (*a*) Electron spin resonance (E.S.R.) spectrum of a frozen solution of rubidium HMPA (77 K). The resonance at $g \sim 4$ arises from trace amounts of paramagnetic impurities in the spectrosil (quartz) tubing. (*b*) E.S.R. spectrum recorded at high machine amplification. The assignment of both rubidium-85 and -87 species is indicated, and the method of labelling is outlined in the text.

and -87 species (see following sections) is indicated in figure 1 (*b*). A detailed analysis and discussion of the central singlet resonance is given elsewhere [13].

4. Analysis of spectra

4.1. *Energy levels and electron spin transitions*

The energy levels $W_{(F,\,m_F)}$ for an atom with $I=\frac{1}{2}$ in an external magnetic field are given by the Breit–Rabi [9] equation

$$W_{(F,\,m_F)}=\frac{-\Delta W}{2(2I+1)}+g_I\mu_B H m_F \pm \frac{\Delta W}{2}\left\{1+\frac{4m_F x}{2I+1}+x^2\right\}^{1/2}, \tag{4}$$

where

$$x=\{(g-g_I)\mu_B H/\Delta W\} \tag{5}$$

and ΔW, the zero-field splitting, is given by

$$\Delta W=ag\mu_B(2I+1)/2, \tag{6}$$

where g_I and g are the nuclear and electronic g-factors, μ_B is the Bohr magneton, H is the external field value and m_F is the total magnetic quantum number (m_I+m_J) associated with the total spin angular momentum of the electron (J) and nuclear (I) spins, respectively.

Energy level diagrams (obtained from equation (4)) for the two naturally occurring isotopes of rubidium (rubidium-87 : $I=\frac{3}{2}$, 27·2 per cent ; rubidium-85 : $I=\frac{5}{2}$, 72·8 per cent) are shown in figure 2. For our experiments at *ca.*

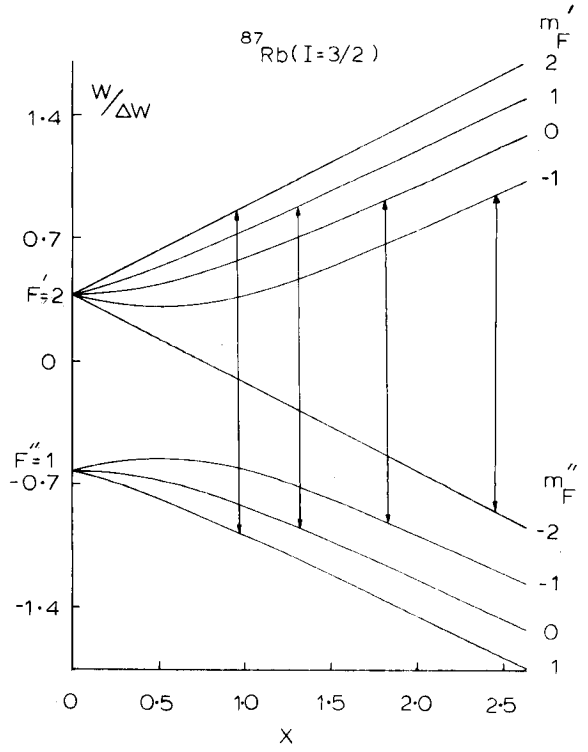

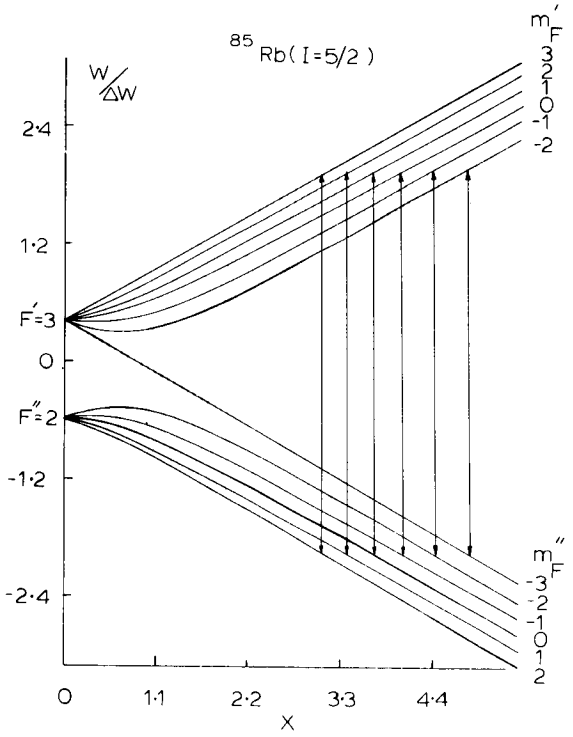

Figure 2. Breit–Rabi magnetic energy levels in an external magnetic field : (*a*) rubidium-87 state ($I=\frac{3}{2}$), $a=850$ G, $g=1{\cdot}9980$; (*b*) rubidium-85 state ($I=\frac{5}{2}$), $a=250$ G, $g=1{\cdot}9980$. The abscissa is the dimensionless parameter x, where $x=(g-g_I)\mu_B H/\Delta W$, which is proportional to the applied magnetic field. Each level is labelled by its ' weak-field ' quantum numbers (F, m_F) where F', m_F' refer to the upper levels and F'', m_F'' refer to the lower levels. The nuclear magnetic moment is assumed positive.

9·1 GHz, the value of the parameter $x(=(g-g_I)\mu_B H/\Delta W)$ in these systems is in the range 3·0–5·0 for the rubidium-85 states, and 0·9–2·5 for the rubidium-87 states. The systems are characterized as being in the low- and intermediate-field regions [2, 3, 9] and magnetic energy levels possess appreciable curvature (figure 2). *Allowed* electron spin transitions (H_1 perpendicular to H ; $\Delta F=\pm 1$, 0 ; $\Delta m_F=\pm 1$) are indicated in figure 2. The curvature in hyperfine levels manifests itself in an increased separation between adjacent members of the multiplet resonances as one moves to higher field values.

4.2. *Estimation of magnetic parameters*

For values of the rubidium-85, -87 hyperfine coupling constant observed in this investigation, higher-order [10 (*a*), (*b*)] (perturbation) analyses lead to erroneous results [11]. Under these circumstances evaluation of magnetic parameters (a, g) for a field-swept E.S.R. experiment requires an iterative solution of the Breit–Rabi equation without any approximations.

The $(2I+1)$ permitted electron spin transitions have been indicated in figure 2. If one takes the difference in energy between two appropriate levels of the same m_I value (high-field notation) but different m_J values, then it is

possible to derive from equation (4) a set of $(2I+1)$ analytical expressions for the frequencies of allowed transitions as a function of the applied magnetic field.

For example, in the case $I=\frac{3}{2}$; the transition frequency $(\delta\nu)$ for the $m_I=-\frac{1}{2}\{(2,0)\leftarrow(1,-1)\}$ resonance is readily computed to be

$$\delta\nu=\frac{1}{h}[W(2,0)-W(1,-1)] \tag{7}$$

giving (from equation (4))

$$\delta\nu=\frac{\Delta W}{h}[\tfrac{1}{2}(1+x^2)^{1/2}+\tfrac{1}{2}(1-x+x^2)^{1/2}+y], \tag{8}$$

where h is Planck's constant and y is defined as $(g_I\mu_B H/\Delta W)$. The frequencies of allowed electron spin transitions $(\Delta F=\pm1,\ 0;\ \Delta m_F=\pm1)$ for the $I=\frac{5}{2}$, $J=\frac{1}{2}$ case (not previously given in the literature†) are presented analytically in table 1 and are plotted in figure 3 for a rubidium-85 species ($a=250{\cdot}91$ G, $g=1{\cdot}99841$) under consideration.

m_I	$(F', m_F')\leftarrow(F'', m_F'')$	Frequency of transition, $\delta\nu$ (sec^{-1})
$\frac{5}{2}$	$(3,3)\leftarrow(2,2)$	$\Delta\nu[\frac{1}{2}(1+x)+\frac{1}{2}(1+\frac{4}{3}x+x^2)^{1/2}+y]$
$\frac{3}{2}$	$(3,2)\leftarrow(2,1)$	$\Delta\nu\left[\frac{1}{2}(1+\frac{4}{3}x+x^2)^{1/2}+\frac{1}{2}\left(1+\frac{2x}{3}+x^2\right)^{1/2}+y\right]$
$\frac{1}{2}$	$(3,1)\leftarrow(2,0)$	$\Delta\nu\left[\frac{1}{2}\left(1+\frac{2x}{3}+x^2\right)^{1/2}+\frac{1}{2}(1+x^2)^{1/2}+y\right]$
$-\frac{1}{2}$	$(3,0)\leftarrow(2,-1)$	$\Delta\nu\left[\frac{1}{2}(1+x^2)^{1/2}+\frac{1}{2}\left(1-\frac{2x}{3}+x^2\right)^{1/2}+y\right]$
$-\frac{3}{2}$	$(3,-1)\leftarrow(2,-2)$	$\Delta\nu\left[\frac{1}{2}\left(1-\frac{2x}{3}+x^2\right)^{1/2}+\frac{1}{2}\left(1-\frac{4x}{3}+x^2\right)^{1/2}+y\right]$
$-\frac{5}{2}$	$(3,-2)\leftarrow(3,-3)$	$\Delta\nu\left[\frac{1}{2}\left(1-\frac{4x}{3}+x^2\right)^{1/2}-\frac{1}{2}(1-x)+y\right]$

Frequencies of allowed E.S.R. transitions computed from the Breit–Rabi equation (equation 4): $\Delta\nu=\Delta W/h$; $x=(g-g_I)\mu_B H/\Delta W$; $y=g_I\mu_B H/\Delta W$.

Table 1. Frequencies of allowed E.S.R. transitions $(\Delta F=\pm1,0;\ \Delta m_F=\pm1)$ for states with $I=\frac{5}{2}$, $J=\frac{1}{2}$.

Expressions of the type (8) provide a method for determining a and g from the experimental observations $[H_{exp},\ \nu_{exp}]$. By equating the calculated and experimental transition frequencies, one can interpolate to evaluate the $(2I+1)$ resonant field positions for a given value of a and g (figure 3). A comparison of experimental and calculated line positions in a weighted least-squares sense [11, 12] then leads to *one* point on a least-squares surface. Repeated iteration

† The frequencies of transitions between magnetic sublevels of atoms with $J=\frac{1}{2}$ and $I=\frac{1}{2}$, 1 and $\frac{3}{2}$ have been given previously, see reference [3], p. 89.

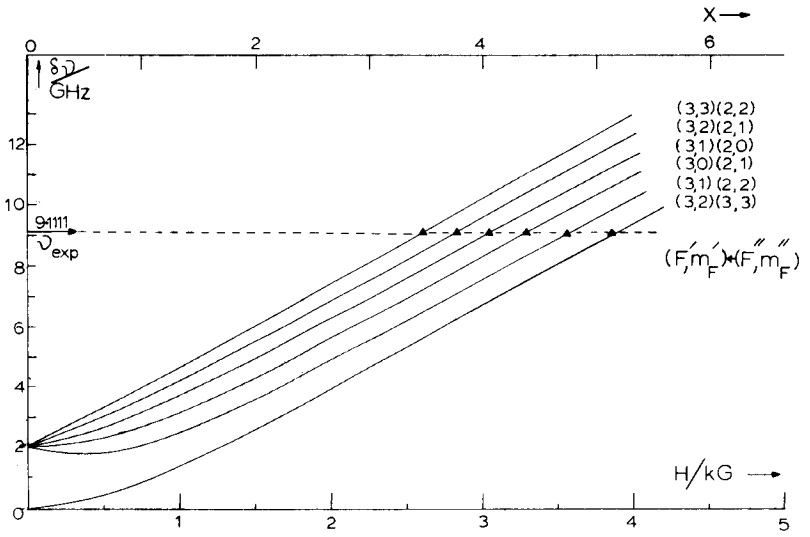

Figure 3. The frequencies of allowed E.S.R. transitions ($\Delta F = \pm 1, 0$; $\Delta m_F = \pm 1$) between magnetic sublevels ($J = \frac{1}{2}$, $I = \frac{5}{2}$) plotted as a function of the external magnetic field and the x parameter, where $x = (g - g_I)\mu_B H/\Delta W$. The points are experimental values taken from the E.S.R. spectrum of the $^{85}M_G$ species at 113 K (table 2). The curves represent the calculated transition frequencies (equation (4) and table 1) for a rubidium-85 centre with $a = 250{\cdot}91$ G; $g = 1{\cdot}99841$ (table 2). A comparison of experimental and calculated line positions for an experimental frequency (9·1111 GHz in this instance) and given values of a and g form the basis of the Breit–Rabi analysis of the magnetic resonance data (see text and table 2).

over a range of a and g-factors leads ultimately to a complete least-squares surface, and the minimum on such a surface represents the values of the magnetic parameters (a, g) which best describe the observed spectrum.

A least-squares surface, obtained from a typical rubidium-85 analysis after 13 iteration loops, is shown in figure 4. The corresponding calculated line

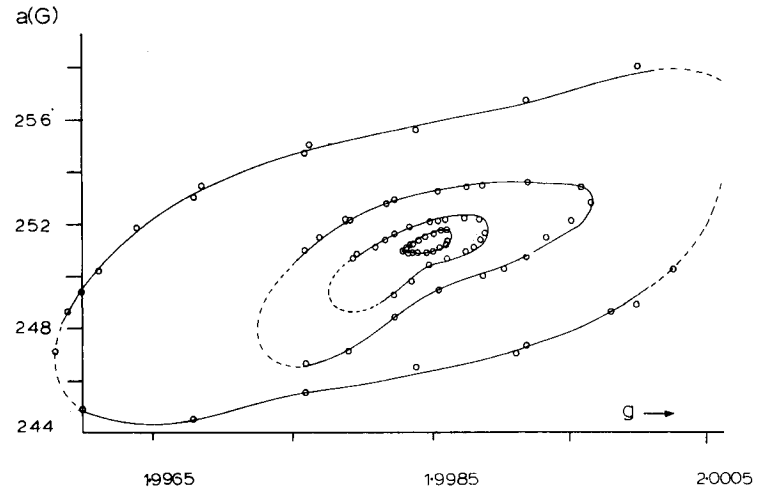

Figure 4. A least-squares surface generated from an analysis of a rubidium-85 spectrum. (Species $^{85}M_G$, 145 K, table 2).

Species	T/K		^{85}Rb line-positions $+\frac{5}{2}$ (3, 3) ← (2, 2)	$+\frac{3}{2}$ (3, 2) ← (2, 1)	$+\frac{1}{2}$ (3, 1) ← (2, 0)	$-\frac{1}{2}$ (3, 0) ← (2, −1)	$-\frac{3}{2}$ (3, −1) ← (2, −2)	$-\frac{5}{2}$ (3, −2) ← (3, −3)	a/G	g
$^{85}M_G$ (*a*) (*c*)	113	Obs./G (*b*)	2606·6	2816·7	3048·1	3299·3	3570·9	3860·3	250·91	1·99841
		Err./G	3	0·5	0·5	0·3	0·4	0·8		
		Calc./G	2604·8	2816·7	3048·1	3299·4	3570·5	3858·1		
		ν/GHz	←			9·1111		→		
$^{85}M_G$ (*d*)	145	Obs./G	2600·9	2813·6	3045·5	3298·1	3570·2	3862·7	251·93	1·99846
		Err./G	0·4	0·4	0·2	0·2	0·2	0·4		
		Calc./G	2600·5	2813·2	3045·8	3298·1	3570·3	3862·2		
		ν/GHz	9·1073	9·1074	9·1083	9·1084	9·1083	9·1082		

(*a*) Nomenclature defined in the text. (*b*) Obs. (observed); Err. (estimated error (G) in observed line position); Calc. (calculated); all values in G (1 G ≡ 0·1 mT). (*c*) See figure 2. (*d*) A least-squares surface for this analysis is given in figure 4.

Table 2. Magnetic parameters derived from the E.S.R. spectra of frozen solutions of rubidium in HMPA (sample Rb–1, Pyrex vessel); representative results from a full Breit–Rabi analysis of experimental data.

positions are compared with experimental values in table 2 (species $^{85}M_G(P)$; 145 K, see next section).

4.3. *Magnetic parameters*

We have identified *both* rubidium-85 and rubidium-87 resonances from two, high atomic-character states [13] in these frozen rubidium–HMPA glasses (figure 1 (*b*)). Several more rubidium-85 resonances have been characterized [13]. However, the low relative concentrations of these states (see, for example, figure 13 of reference [13]), coupled with the low natural abundance of the rubidium-87 isotope, have precluded the identification of the corresponding -87 resonances.

On a provisional system of identification [13], we have classified states in terms of their percentage occupancy of the rubidium-5*s* orbital; labelling alphabetically from the lowest atomic character state ($^{85}M_A$, *ca.* 1 per cent) to the highest ($^{85}M_I$, *ca.* 80 per cent). Superscripts denote the mass number of the particular isotope.

Figure 1 (*b*) shows our identification of resonances from the $^{85,87}M_G$ and $^{85,87}M_D$ states, and table 3 gives a full listing of derived magnetic parameters.

Values of the rubidium-85, -87 hyperfine structure anomaly were calculated from

$$ {}_{85}\Delta_{87} = \frac{(a_{85}/a_{87})_{\text{obs.}} - (a_{85}/a_{87})_{\text{calc.}}}{(a_{85}/a_{87})_{\text{calc.}}}, \tag{9} $$

where

$$ \left(\frac{a_{85}}{a_{87}}\right)_{\text{calc.}} = \left(\frac{\mu_I(85)}{\mu_I(87)}\right) \times \left(\frac{I_{87}}{I_{85}}\right) \tag{10} $$

and in table 3 we compare values of ${}_{85}\Delta_{87}$ obtained from our solid-state studies with experimental gas-phase values. All analyses of the solid-state data gave positive values for ${}_{85}\Delta_{87}$. Average values were $(1{\cdot}672 \pm 0{\cdot}8) \times 10^{-3}$ for four observations (two samples, 77–145 K) of the $^{85,87}M_G$ species (70 per cent atomic character) and $(5{\cdot}7 \pm 2{\cdot}0) \times 10^{-3}$ for two observations (two samples, 77 K) of the $^{85,87}M_D$ species (60 per cent atomic character). The quoted error is the average deviation taken over the total number of runs.

5. Discussion

5.1. *Origins of the hyperfine structure anomaly in isolated (gas-phase) atoms*

A non-zero value for the hyperfine structure anomaly arises because of the finite size and mass of the nucleus. The latter effect leads to a reduced-mass correction term [2, 3] in the Fermi–Sergé formula (2), such that

$$ \frac{a_1}{a_2} = \left(\frac{\mu_{I_1}}{\mu_{I_2}}\right)\left(\frac{I_2}{I_1}\right)\left(\frac{m_1}{m_2}\right)^3, \tag{11} $$

where m_1 and m_2 are the reduced masses for the two isotopes. For one-electron atoms in the *S*-state, m_1 and m_2 are taken [2] as the reduced-mass of the *ns*-electron in atoms 1 and 2 respectively. However, for multi-electron atoms

$$ (m_1/m_2) \sim 1 \tag{12} $$

Species (-sample) (*a*)	*T*/K	^{85}Rb $\Delta g \times 10^4$	^{85}Rb *a*/G	^{85}Rb Per cent a.c.	^{87}Rb $\Delta g \times 10^4$	^{87}Rb *a*/G	^{87}Rb Per cent a.c.	$_{85}\Delta_{87} \times 10^3$	References
$^{85,\ 87}M_G$(P)	77	+42·5	251·34	69·61	+42·9	849·00	69·63	+3·285	(*b*)
$^{85,\ 87}M_G$(q)	77	+41·2	253·04	70·08	+31·9	857·03	70·29	+0·607	(*b*)
$^{85,\ 87}M_G$(P)	113	+39·0	250·91	69·49	+44·1	849·36	69·66	+1·144	(*b*)
$^{85,\ 87}M_G$(P)	145–147	+38·5	251·93	69·77	+32·7	852·38	69·90	+1·653	(*b*)
			Average value $(_{85}\Delta_{87}) = (1{\cdot}672 \pm 0{\cdot}8) \times 10^{-3}$						
$^{85,\ 87}M_D$(P)	77	+38	210·0	58·2	+37	706·3	57·9	+7·63	(*b*)
$^{85,\ 87}M_D$(q)	77	+35	212·8	58·9	+51	718·4	58·9	+3·86	(*b*)
			Average value $(_{85}\Delta_{87}) = (5{\cdot}7 \pm 2{\cdot}0) \times 10^{-3}$						
Gas-phase (obs.)	—	−10·0	361·063	100	−10·0	1219·350	100	3·515 ±0·004	[5, 6]
Gas phase (obs.)	—	−7·0	361·068	~100	−7·0	1219·368	~100	3·517	(*c*)
			Gas-phase value $(_{85}\Delta_{87}) = (3{\cdot}515 \pm 0{\cdot}004) \times 10^{-3}$						

(*a*) Sample prepared and examined in Pyrex (P) or quartz (q) vessel. (*b*) This work. (*c*) Calculated from experimental results of reference [7].

Table 3. The rubidium-85, -87 hyperfine structure anomaly in gaseous and matrix-bound rubidium atoms.

and the principal contribution to a non-zero value for ${}_1\Delta_2$ arises from the finite size of a nucleus [3].

A nucleus of finite size will give rise to a spatial distribution of the magnetic dipole over the nuclear volume, and a distortion of the electronic wavefunction at distances less than the nuclear radius. It is therefore necessary to average the factor $(\mu_I|\psi(0)|^2)$ in equation (1) over the entire nuclear volume so that the resultant hyperfine splitting will depend on the nuclear charge, the nuclear size and the spatial distribution of the magnetic moment over the nucleus, such that [15]

$$a_{\text{obs.}} = \frac{8\pi}{3}\left(\frac{\mu_I}{I}\right)\mu_N|\psi(0)|^2\{(1+\epsilon_{\text{RB}})(1+\epsilon_{\text{BW}})\} \tag{13}$$

where

$$\{(1+\epsilon_{\text{RB}})(1+\epsilon_{\text{BW}})\} = \frac{\langle\mu_I(r)|\psi(r)|^2\rangle_{\text{av.}}}{\mu_I|\psi(0)|^2} \tag{14}$$

The factor $(1+\epsilon_{\text{RB}})$ takes into account the Rosenthal–Breit [15, 16] effect arising from the departure of the electronic wavefunction from that for a pure Coulomb (point–dipole) field at positions within the nucleus. The Rosenthal–Breit correction is generally many times smaller than the so-called Bohr–Weisskopf correction (ϵ_{BW}) and to a good approximation, $\{(1+\epsilon)_{\text{RB}}(1+\epsilon_{\text{BW}})\} \simeq (1+\epsilon_{\text{BW}})$.

The Bohr–Weisskopf correction factor $(1+\epsilon_{\text{BW}})$ is a direct consequence of the spatial distribution of the magnetic dipole in a nucleus [17]. The existence of a distribution in the nuclear magnetism was first suggested by Kopfermann [18] and Bitter [4] before being computed directly by Bohr and Weisskopf [17]. The effect gives rise to a hyperfine interaction when the electron is inside the nucleus, and changes in the distribution of the nuclear magnetism between isotopes of the same electronic state lead to significant anomalies in the hyperfine coupling constant. The quantity ϵ_{BW} is related to the rubidium-85, -87 hyperfine structure anomaly by

$${}_{85}\Delta_{87} = \epsilon_{\text{BW}}({}^{85}\text{Rb}) - \epsilon_{\text{BW}}({}^{87}\text{Rb}). \tag{15}$$

Bohr and Weisskopf [17] assumed a spherically symmetrical magnetic moment distribution and found

$$\epsilon_{\text{BW}} = (\alpha_s + 0{\cdot}62\,\alpha_L)b\langle R^2/R_0^2\rangle_{\text{av.}}, \tag{16}$$

where α_s and α_L are, respectively, the fractions of the nuclear magnetic moment due to the spin and orbital angular momentum, b is a parameter dependent only upon z and R_0 (the nuclear radius) and $\langle R^2\rangle_{\text{av.}}$ is the mean square radius of the nucleus or nucleous producing the magnetization. The computed value [17] $(2{\cdot}9\times10^{-3})$ for the gas-phase rubidium-85, -87 anomaly $({}_{85}\Delta_{87})$ is in reasonable agreement with the experimental value [5, 6] $(3{\cdot}515\pm0{\cdot}004)\times10^{-3}$.

5.2. *The rubidium*-85, -87 *solid-state hyperfine structure anomaly*

Values of ${}_{85}\Delta_{87}$ derived from our solid-state results are given in table 3. Results from analyses of both the ${}^{85,87}\text{M}_{\text{G}}$ and ${}^{85,87}\text{M}_{\text{D}}$ E.S.R. spectra gave positive values for ${}_{85}\Delta_{87}$, in agreement with gas-phase values.

Two aspects of the solid-state results merit attention :

(i) numerical values for $_{85}\Delta_{87}$ in both the $^{85,87}M_G$ and $^{85,87}M_D$ species are in reasonable *overall* agreement with the gas-phase value (that is, both values are of the order of 10^{-3}) ;

(ii) a closer examination of results for the $^{85,87}M_G$ specise (for which intrinsic errors in $_{85}\Delta_{87}$ are *ca.* one-third of those for the corresponding $^{85,87}M_D$ analyses) shows that the solid-state values for $_{85}\Delta_{87}$ consistently fall below the gas-phase value.

With regard to (i), the *overall* agreement between results for the two phases is particularly striking when one considers that for the solid-state species *ca.* 30–40 per cent of the unpaired electron is delocalized onto the surrounding medium as a result of dielectric shielding of the parent-ion (Rb^+) unpaired-electron Coulomb interaction [13]. A discussion of possible solid-state effects on the hyperfine structure anomaly has been given by Eisinger and Feher [19]. These authors make the important point that the detailed behaviour of the unpaired electron *outside* the nucleus is of little consequence in any consideration of the anomaly. The hyperfine interaction occurs when the electron is *inside* the nucleus and its (the electron's) behaviour in these circumstances will be the same irrespective of whether the atom is in the gas phase or embedded in the host (HMPA) matrix.

With regard to point (ii), it is instructive to compare the sign, and magnitude, of the electronic g-factor shifts ($\Delta g = 2{\cdot}00231 - g$) for gaseous and matrix-bound states.

For isolated (gas-phase) rubidium atoms, the dominant spin–orbit interaction occurs well inside the ion-core [8, 11 (b), 20], and the deep lying *filled* (4p) states *below* the valence state (5*s*) dictate the magnitude of the slight g-shift, such that $g(^{85,87}\text{Rb, gaseous}) = 2{\cdot}002409$; $\Delta g = -0{\cdot}99 \times 10^{-3}$. In contrast, matrix-bound rubidium-85, -87 states have g-factors below the free-spin value [typically : ($^{85}M_G$), $g = 1{\cdot}99806$, $\Delta g = +42{\cdot}5 \times 10^{-3}$] such that the dominant spin–orbit interaction mixes *higher*, *unoccupied*, 5p-states into the ground state [8]. The large g-factor shifts (table 3) suggest a reasonable admixture of these higher angular momentum ($L > 0$) states into the ground state [21]†.

It is well established that for pure p, d, f (i.e. $L > 0$) electron states, the finite size of a nucleus and/or the distribution of nuclear magnetism have negligible effect on the hyperfine structure [2, 3]. The reason is simply that for these states the electron wavefunction is vanishing at the nucleus, that is, $|\psi(0)|^2 = 0$. We propose that the spin–orbit admixture of some 5p-character into the 5*s*-like ground-state wavefunction of the matrix-bound states is responsible for the decrease in $_{85}\Delta_{87}$ on moving from the isolated- to impurity-atom situations.

In conclusion, we would again comment on the encouraging overall agreement between values of the hyperfine structure anomaly determined by electron spin resonance spectroscopy and by conventional molecular beam studies. The Breit–Rabi equation (equation (4)) refers to a constant-field, frequency-swept (atomic-beam) experiment and can therefore be used *directly* to extract a and

† The role played by local (short-range) structure in determining the observed g-factor for an impurity state (Fe^{3+}) in glass has been discussed in reference [21]. We are grateful to one of the referees for bringing this publication to our notice.

hence the hyperfine structure anomaly. In contrast, the analysis of a constant-frequency (field-swept) electron spin resonance experiment requires an iterative, *indirect*, approach to evaluate a. The numerical techniques outlined in this report appear quite adequate in this respect and should be helpful in establishing a possible use of E.S.R. in probing the nuclear structure of states in which conventional (gas-phase) atomic-beam spectroscopy is inapplicable.

We thank the S.R.C. for financial support. Part of this report was prepared while one of us (P.P.E.) was engaged on a National Science Foundation Post-doctoral Fellowship at Cornell University. We would also like to thank Professor M. J. Sienko for his hospitality to Peter Edwards during this period.

References

[1] Fermi, E., and Segrè, E. G., 1933, *Z. Phys.*, **82,** 729.
[2] Ramsey, N. F., 1956, *Molecular Beams* (Oxford University Press).
[3] Kusch, P., and Hughes, V. W., 1959, *Encyclopedia of Physics*, Vol. XXXVII/I, edited by S. Flügge (Springer-Verlag).
[4] Bitter, F., 1949, *Phys. Rev.*, **76,** 150.
[5] Ochs, S. A., and Kusch, P., 1952, *Phys. Rev.*, **85,** 145.
[6] Daly, Jr., R. T., and Zacharias, J. R., 1953, *Phys. Rev.*, **91,** 476.
[7] De Lange, C. A., and Monster, A. A., 1972, *Chem. Phys. Lett.*, **13,** 561.
[8] Catterall, R., and Edwards, P. P., 1976, to be published in *Trans. Faraday Soc.*
[9] Breit, G., and Rabi, I. I., 1931, *Phys. Rev.*, **38,** 2082.
[10] (a) Bleaney, B., 1951, *Phil. Mag.*, **42,** 441. (b) Fessenden, R. W., and Schuler, R. H., 1965, *J. chem. Phys.*, **43,** 2704.
[11] (a) Catterall, R., and Edwards, P. P., 1976, to be published. (b) Edwards, P. P., 1974, Ph.D. Thesis, Salford University (unpublished).
[12] Topping, J., 1956, *Errors of Observation and their Treatment* Monograph for Students (Institute of Physics).
[13] Catterall, R., and Edwards, P. P., 1975, *J. phys. Chem.*, **79,** 3010.
[14] Eisinger, J. T., Bederson, B., and Feld, B. T., 1952, *Phys. Rev.*, **86,** 73.
[15] Rosenthal, J. E., and Breit, G., 1932, *Phys. Rev.*, **41,** 459.
[16] Racah, G., 1932, *Nature, Lond.*, **129,** 723.
[17] Bohr, A., and Weisskopf, V. F., 1950, *Phys. Rev.*, **77,** 94.
[18] Kopfermann, H., 1940, *Kernmomente* (Akademische Verlagsgesellschaft, M.B.H., Leipzig).
[19] Eisinger, J., and Feher, G., 1958, *Phys. Rev.*, **109,** 1172.
[20] Yafet, Y., 1963, *Solid State Physics*, Vol. 14, edited by F. Seitz, and D. Turnbull (Academic Press, New York).
[21] Castner, T., Newell, G. S., Holton, W. C., and Slichter, C. P., 1960, *J. chem. Phys.*, **32,** 668.